4-27-2021

Feedstock Processing for Extraterrestrial Metal Additive Manufacturing

Japheth A. Hayman

Feedstock processing for extraterrestrial metal additive manufacturing

by

Japheth A. Hayman

An Honors Capstone

submitted in partial fulfillment of the requirements

for the Honors Diploma

to

The Honors College

of

The University of Alabama in Huntsville

April 27, 2021

Honors Capstone Director: Dr. Judy Schneider

Professor of Mechanical and Aerospace Engineering

Student	April 26, 2021 Date
Director	April 26, 2021 Date
Department Chair	4/26/2021 Date
Honors College Dean	William Wilkerson Digitally signed by William Wilkerson Date: 2021.04.28 09:50:13 -05'00' Date

Honors College
Frank Franz Hall
+1 (256) 824-6450 (voice)
+1 (256) 824-7339 (fax)
honors@uah.edu

Honors Thesis Copyright Permission

This form must be signed by the student and submitted as a bound part of the thesis.

In presenting this thesis in partial fulfillment of the requirements for Honors Diploma or Certificate from The University of Alabama in Huntsville, I agree that the Library of this University shall make it freely available for inspection. I further agree that permission for extensive copying for scholarly purposes may be granted by my advisor or, in his/her absence, by the Chair of the Department, Director of the Program, or the Dean of the Honors College. It is also understood that due recognition shall be given to me and to The University of Alabama in Huntsville in any scholarly use which may be made of any material in this thesis.

Japheth Hayman

Student Name (printed)

Student Signature

04/26/21

Date

Table of Contents

Abstract

There is currently great interest, both from private industry and government organizations such as the National Aeronautics and Space Administration (NASA), in human occupation and exploration of outer space. This push necessitates the development of an infrastructure network by which humans may travel safely away from Earth. Economical space travel will require the ability to manufacture and repair systems during extraterrestrial missions. Such repairs will require the manufacture of individual metal parts in environments far from terrestrial foundries and factories. To support these efforts, the viability of various manufacturing methods for lunar and other extraterrestrial applications is being evaluated. In particular, additive manufacturing is being investigated for its modularity and minimal waste, in addition to the ability to utilize in-situ resources. Of the many metal additive manufacturing processes, the methods that utilize metal powders as feedstock appear most amenable to remote environments. This study considers two powder-based additive manufacturing processes for an extraterrestrial environment. Iron, a plentiful material in space and an important structural metal on Earth, was chosen as the substrate for which extraterrestrial additive manufacturing techniques may be developed. This study also evaluates ball milling as a method of processing feedstock and the suitability of different morphologies for different additive processes. Major findings from this study indicate that electrochemically extracted iron may be directly suitable for laser powder bed fusion, but may require additional pre-processing for use in laser powder direct energy deposition. This pre-processing would involve high-energy ball milling or other novel powder refinement techniques.

I. Background

It is presently of great interest to the scientific community to further explore outer space. In order to send manned missions beyond Earth's moon, or to more efficiently send unmanned missions to extrasolar space, a low-gravity launch site must be developed. To this end, the National Aeronautics and Space Administration (NASA) is developing plans for the construction of a lunar "base camp" capable of habitation, launch, and repair (NASA 2019). Such a facility necessitates metal manufacturing capabilities. However, most terrestrial manufacturing methods for metals require bulky infrastructure, which must be transported from Earth. Since the size and volume of the manufacturing equipment is severely limited by the payload capacity of launch vehicles, a small, modular solution is preferred. Further, primary manufacturing processes, such as smelting and casting, require containment of molten metals, which largely relies on gravity. Given the relatively low gravitational pull of the Moon, paired with the necessary compactness of the lunar facility, attempting to contain any significant volume of molten metal poses an immediate safety risk. Additive manufacturing may solve the issues of infrastructure and containment.

There is currently a multitude of different methods under the umbrella of metal additive manufacturing, as illustrated in Figure 1. In general, these methods can be categorized by the use of either a metal powder or a wire as feedstock. Manufacturing of wire for feedstock would require containment of molten metal prior to drawing, which require a series of bulky dies. In contrast, the use of powder feedstock can utilize in-situ resources already found throughout our solar system. Meteoroids are a known source of extraterrestrial iron, which is the most common structural metal to date. Meteorites, which are meteoroids that have landed on another

astronomical body, can be gathered from impact craters on the Moon. There is also potential for catching meteoroids in space.

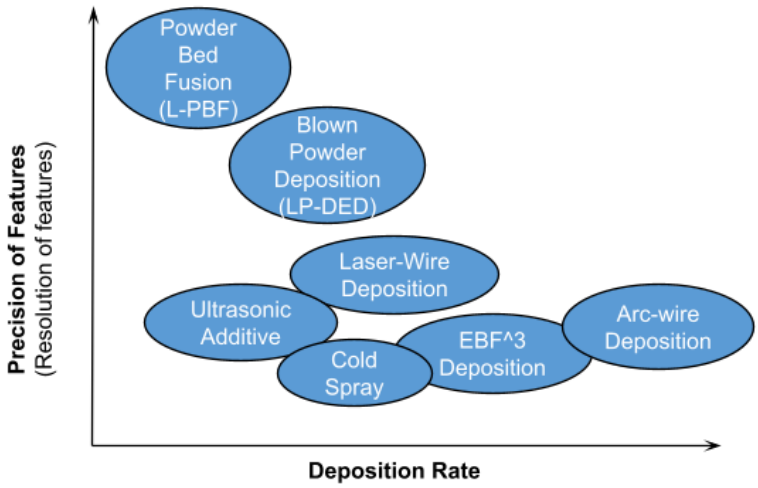

Figure 1 – Additive manufacturing processes present a tradeoff between deposition speed and feature resolution.

Due to its relative recency, additive manufacturing tends to utilize feedstock developed for other processes – wires are picked from materials in production for welding, and powders are chosen from powder metallurgy feedstock. While there are known criteria for selecting feedstock from available materials, research is only beginning to optimize a feedstock specifically for additive manufacturing (Anderson, White and Dehoff 2018). Currently, there is some question as to whether the spheroidal powders developed for powder metallurgy are optimal for powder-based additive processes (Field, et al. 2020).

This study focuses on two powder-based additive manufacturing processes: laser powder bed fusion (L-PBF) and laser powder direct energy deposition (LP-DED). These additive manufacturing processes were selected as candidates for lunar applications because of their low reliance on gravity. LP-DED utilizes a pressure gradient to move powders, and L-PBF has

recently been demonstrated to work in microgravity using a vacuum to contain the powder (Zocca, et al. 2014).

L-PBF involves depositing a layer of powder that covers a bed, selectively melting some of the powder with a laser as illustrated in Figure 2. These micron-sized selective areas undergo rapid melting and solidification. As a layer is completed, the process repeats with another layer of powder. For this reason, regardless of the shape or size of the final part, the entire bed is filled with powder, up to the height of the part. Although this results in excess powder, which can be processed for reuse, it requires a dose chamber filled with powder at the start of the process. In contrast, since LP-DED delivers powder from a hopper to the laser focal point, less powder is required at the start of a build. Figure 3 illustrates how the powder is blown through a coaxial nozzle towards the substrate material using an inert carrier gas. The axially aligned laser melts the powder as it arrives at the substrate. This laser-nozzle system scans along the shape of the component, with the metal solidifying as it is deposited, continuously building up additional layers.

Due to the difference in delivery, suitable powder morphology and size may vary between the two processes (Goh, Heng and Liew 2018). The LP-DED process relies on powder flowing steadily, while the L-PBF requires packing of the powders. Several shape characteristics, namely size and various “roundness” indicators, have been determined to be major factors influencing the flowability and packing characteristics of powders (Yu, et al. 2011, Fu, et al. 2012). Ball milling was identified as a viable process for modifying metal powder morphology (Rofman, et al. 2019).

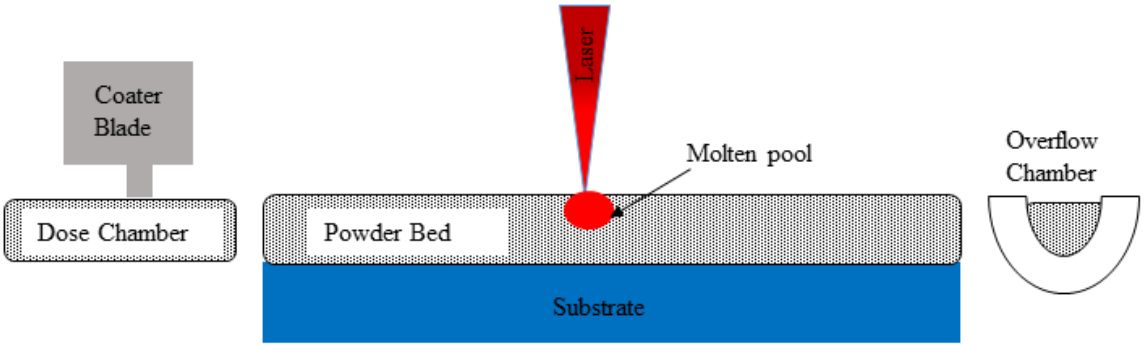

Figure 2 – L-PBF process diagram.

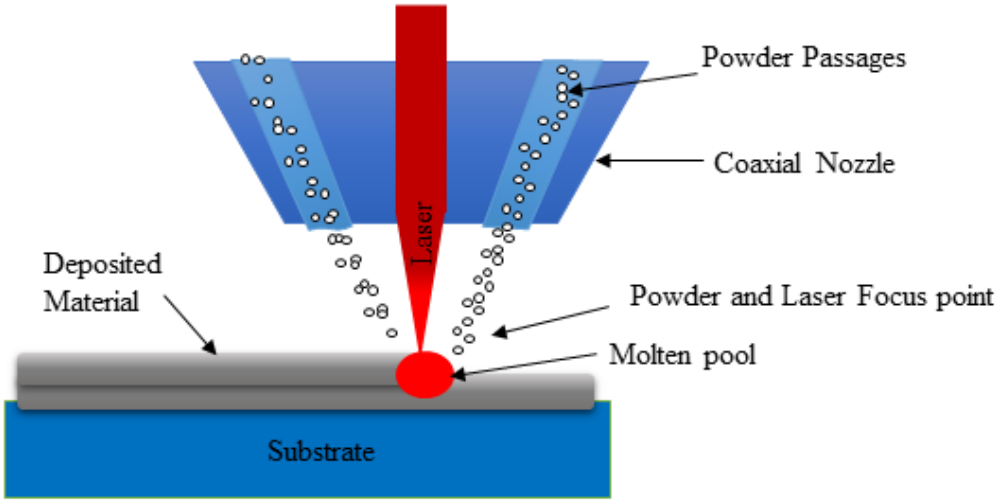

Figure 3 – LP-DED process diagram.

II. Methodology

To extract pure Fe from a meteorite, the specimen is chemically digested, followed by selective electroplating, which yields irregular flakes. Due to the very limited amount of meteorites accessible on Earth, this study uses a simulant of iron flakes similar in morphology to those obtained in the electroplating process. To modify the morphology of the extracted powder, the Fe flakes were ball milled in low vacuum, using a FlackTek Speedmixer model DAC 600.1-LR with ball milling inserts. Steel balls (5 mm diameter) were used in a plastic jar with rounded corners. Five grams of powder were combined with ten grams of mixing balls and pumped to a vacuum of 1/3 atmosphere to reduce oxidation. Flakes were milled at 2000 rpm in 30-second intervals, for a total of three minutes.

The morphology of the extracted powder before and after milling, along with a reference sample of spherical Inconel 625, was characterized using a Zeiss XioVert.A1m Inverted Microscope to obtain optical microscopy images. These images were analyzed using ImageJ to obtain an area-equivalent diameter, aspect ratio and circularity, as illustrated in Figure 4. Hall flow rate was also measured by passing the powder through a Hall flowmeter, seen in Figure 5, per ASTM Standard B-213 (ASTM 2020).

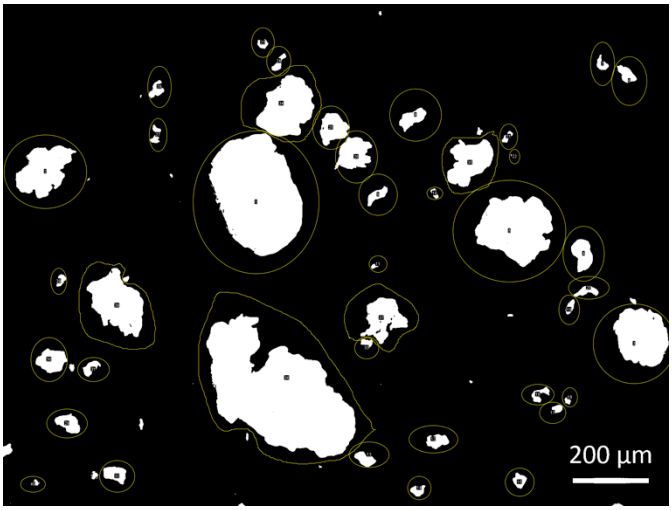

Figure 4 – Ball-milled Fe particles identified for analysis.

Figure 5 – Apparatus for determining Hall flow rate.

Elemental composition of the lighter elements used combustion for carbon and inert gas fusion (IGF) for oxygen and nitrogen per ASTM E1019 (ASTM 2018). The Fe content was not analyzed, using the balance as the composition. Based on the characterization of the extracted

Fe, a simulant of -200 mesh Fe powder (99+% purity) was obtained, favoring comparable morphology over identical composition.

A sample of unprocessed simulant was sent to the NASA Marshall Space Flight Center (NASA-MSFC) for L-PBF processing, yielding a specimen in the shape of a tensile dogbone (Figure 9). Ball-milled simulant was sent to DM3D Technology for LP-DED processing, yielding several loaf-shaped specimens (Figure 10).

Quasi-static tensile testing was conducted on the L-PBF specimen using a modified form of the procedure detailed in ASTM Standard E8 (ASTM 2016). The specimen was modeled after a subsize specimen per section 6.2, with grip sections shortened by 70% to minimize powder usage. An Instron 5985 load frame with a 250 kN load cell was used in displacement control with a constant crosshead velocity of 1.27 mm/min (0.05 in/min), in accordance with the standard. The length alteration was offset by gripping the specimen with spacers, in order to keep grips parallel and loads distributed. Hardness tests were conducted on all samples using a Rockwell B scale per ASTM Standard E18 (ASTM 2020).

Samples from both additive processes were prepared for optical microscopy. Specimens were mounted in two orientations to characterize the build plane and build direction. A section was removed from the grip end of the L-PBF specimen after tension testing. Based on visual inspection, only the least porous specimen from the L-BPD process was sectioned. After mounting the specimens in a phenolic, standard metallographic grinding and polishing procedures were followed with a final polish using an aqueous suspension of 0.05-micron alumina powder. To examine the resulting grain structure, the samples were etched by immersion in Waterless Kalling's Reagent for 20 seconds each.

III. Results

Powder Characteristics

Elemental analysis of the electrochemically-extracted powder is shown in Table 1. Impurities were quantified and the remainder was assumed to be Fe.

Table 1: Fe Powder Composition

Element	Weight %
Carbon	1
Sulfur	3
Nitrogen	0.2
Oxygen	15
Iron	80.8 (balance)

Figures 6 and 7 show the simulant Fe flakes before and after ball milling, respectively. A sample of spheroidal Inconel 625, presently used for LP-DED, is given in Figure 8 for comparison.

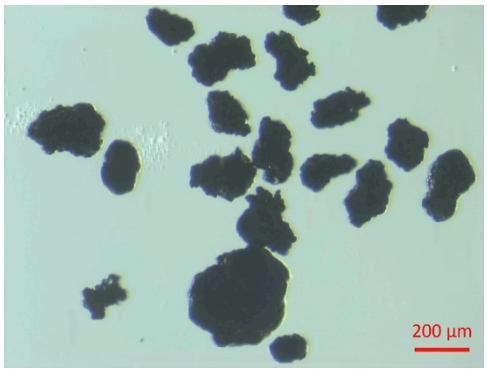

Figure 6 – As-received Fe powder.

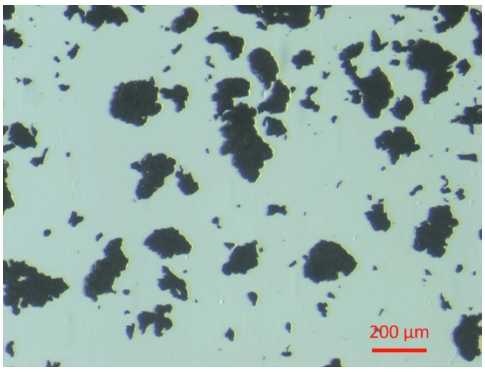

Figure 7 – Ball milled Fe powder.

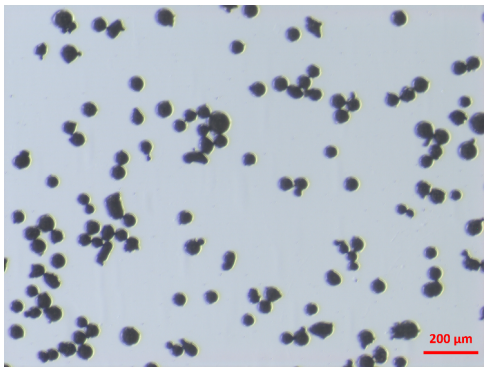

Figure 8 – Reference Inconel 625 spherical powder.

Table 2 characterizes the powders shown in Figures 6-8. Since the particle sizes do not follow a normal distribution, it is only guaranteed that an interval of ±*k* standard deviations from the mean contains the fraction $(k^2 - 1)/k^2$ of the data points, per Chebyshev's inequality. Aspect ratio and circularity tended towards normal distributions, therefore following the better-known 68-95-99.7 rule.

Table 2: Powder Morphology and Flowability

	As-Extracted Fe Simulant	**Ball Milled Fe Simulant**	**Reference Inconel 625**
Diameter (µm)	185 ±155	102 ±150	54 ±34
Aspect Ratio	1.4 ±0.3	1.7 ±0.5	1.2 ±0.3
Circularity	0.73 ±0.12	0.62 ±0.16	0.84 ±0.13
Hall Flow Rate (seconds/50g)	36.3	29.4	12.2

Build Characteristics

Final builds are shown in Figures 9 and 10 for the L-PBF and LP-DED processes, respectively. For the LP-DED processing, a series of 12 specimens shown in Figure 10a were deposited using varying parameters to obtain the densest specimen by visual inspection. Specimen LP-DED-11, the largest and least porous, was selected for further analysis.

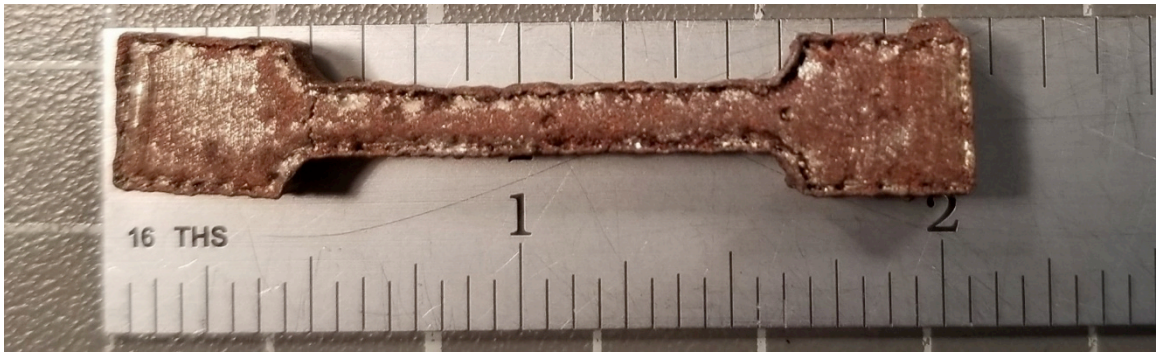

Figure 9 – Specimen L-PBF-1, made from unprocessed Fe powder.

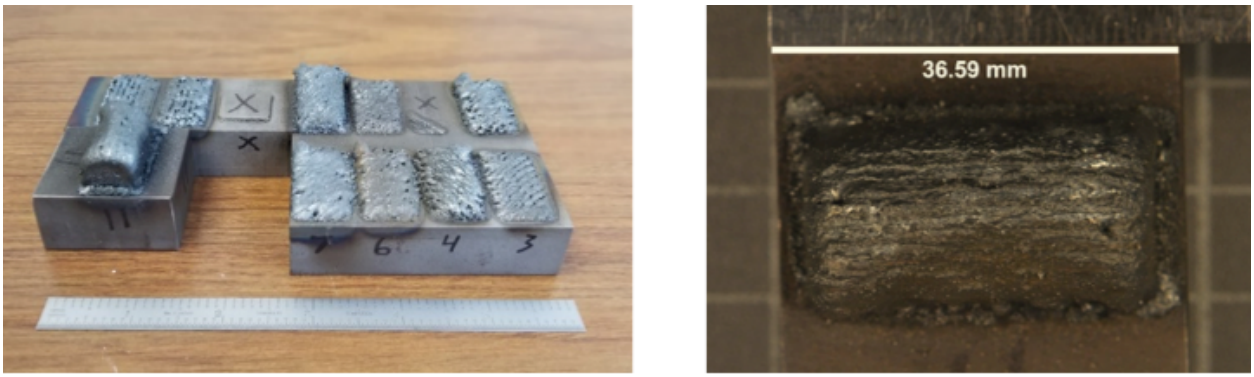

(a) (b)

Figure 10 – (a) LP-DED samples, made from ball-milled Fe powder; (b) Close-up of specimen LP-DED-11.

Table 3 compares the mechanical properties of the two specimens. Standard values for high-purity iron are included for comparison (Cleaves and Hiegel 1942). See Figure 11 for the two orientations used for hardness testing.

Table 3: Mechanical Properties

		L-PBF-1	LP-DED-11	Pure Fe
Yield Strength (ksi)		70.2		6.0 – 7.8
Fracture Elongation (%)		8.7		36 – 46
Ultimate Tensile Strength (ksi)		91.3		78.3
Rockwell Hardness B	**Build Direction**	94.2	56.9 – 69.7	79
	Build Plane	72.7	28.1 – 51.5	

Etched samples of the two specimens are shown in Figure 11. Different shades indicate grain boundaries, due to the random orientation of crystalline structures.

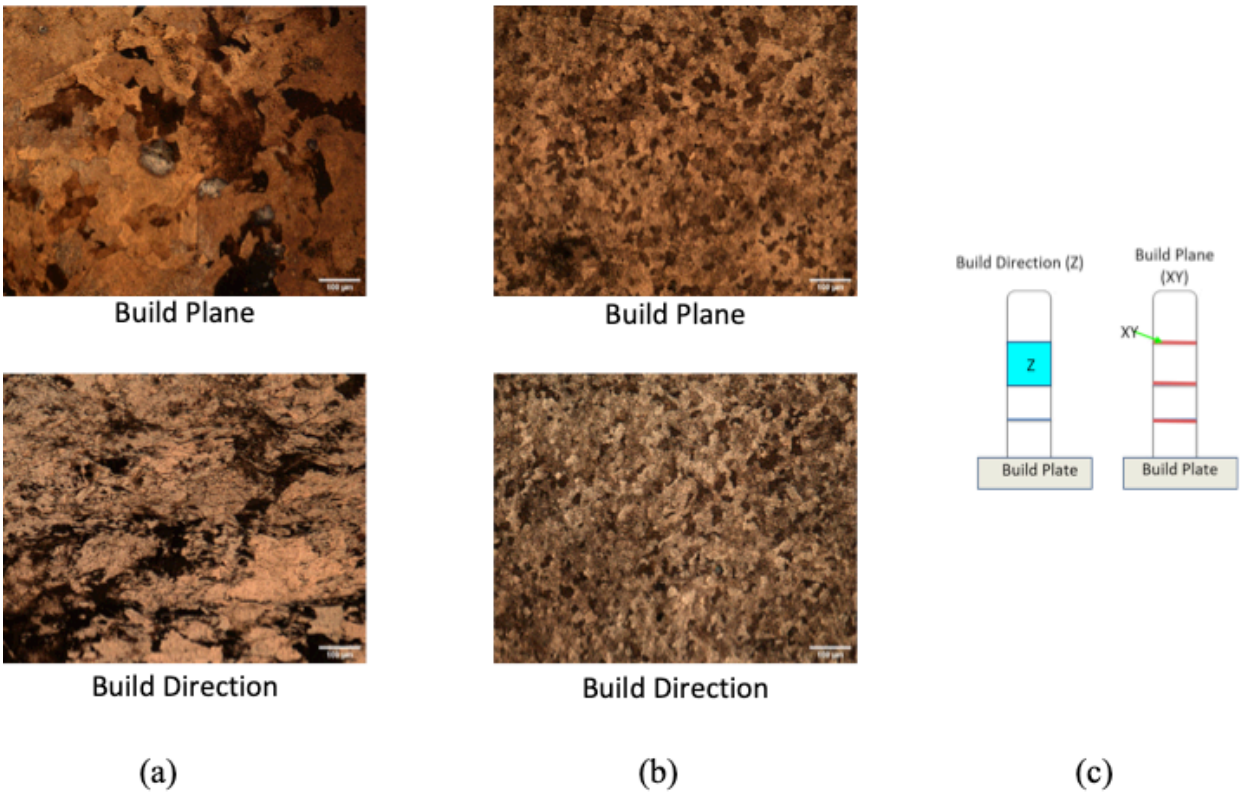

Figure 11 – (a) Microstructure of L-PBF specimen; (b) Microstructure of LP-DED specimen; (c) Orientation of build plane (XY) and build direction (Z) relative to build plate.

IV. Discussion

Table 1 showed the electrochemically processed iron powder was found to have a substantial oxygen content. This is explained by rapid oxidation in Earth's atmosphere due to the high surface area relative to volume. Such an issue is unlikely on the Moon or on other planets, where the presence of oxygen in the atmosphere is much lower than in terrestrial environments. The increased carbon content may be related to the electrochemical processing method, but further investigation is needed. If this is a byproduct of the extraction method, it may be beneficial, as carbon is added to Fe to increase the strength. The extracted iron is chemically more like 1095 steel, a much more commonly used steel alloy for tooling applications, than it is pure Fe.

Due to the 3-dimensional volume and irregularities in particles, characterization of their 2-dimensional morphology is challenging. Many different ratios have been used to quantify the surface smoothness, symmetry, and compactness of shapes and particles, all of which ultimately measure the object's similarity to a circle or sphere. Circularity, most generally, is a measure of roundness for a two-dimensional shape. It is often calculated as the ratio of enclosed area to the area of a circle with the same perimeter. However, for irregular geometries such as those of the powders in this study, this definition of circularity is limited by the resolution of the images used to measure perimeter. Such variance was minimized by instead using the area of a circumscribed circle, based on the major diameter of a fit ellipse. The fit ellipse of a particle is calculated by ImageJ as an ellipse with equal area that covers as much of the particle as possible. This definition of circularity still equals unity for a perfect circle and is therefore believed to be a suitable shape indicator. Using the ellipse fitting method, a substantial spread in diameters for all powders is reflected in the size analysis summarized in Table 2. This spread is noted to increase

after ball milling, in which set a bimodal distribution is observed, with one grouping near the average and a second grouping of much finer particles. The size distribution, paired with the decrease in circularity, indicates that the ball milling process only broke flakes apart, rather than spheroidizing. This is supported by visual comparison of the Fe powder before and after milling with the fully spheroidized reference Inconel (Figure 6, 7, 8). While use of ball milling has been reported as a method to spheriodize particles, it usually is conducted at higher energies than used in this study (Benjamin 1976). Even with retention of the flake morphology, the comparison of Hall flow rates in Table 2 shows that the milled powder flowed more readily than the un-milled powder, though still much slower than the spherical reference.

Due to the small amount of simulant powder available for the L-PBF process, only two samples were printed and only one was mechanically tested. Some warping is noted, as shown in Figure 9. In uniaxial testing of metals, it is assumed that the polycrystalline metal is isotropic, homogenous and continuous. To satisfy this assumption, a representative volume of the metal needs to contain enough randomly oriented grains, which are individually anisotropic, so that the sample's properties are equal to the average of all possible orientations. Although the overall specimen geometry was not in accordance with ASTM standard E8, the gage section geometry was in compliance with the standard and is therefore believed to contain a representative number of grains.

As shown in Figure 10a, several attempts were made at printing a sample with the LP-DED process. The relatively low flowability of the iron powder, even after milling, proved difficult to work with and required several deviations from normal processing parameters. Primarily, DM3D resorted to using a vibrator on the nozzle to encourage powder flow. One persistent effect of the limited flowability was the resulting porosity. This is reflected in the

Rockwell hardness data for LP-DED-11 in Table 3, which is reported as a range because of a large data spread; this spread is due to the presence of large voids within the specimen. L-PBF-1, as compared to pure Fe, has significantly increased yield strength and decreased elongation to fracture. Such differences are common to additive manufacturing processes, as the melting of new layers also reheats previous layers, causing a sort of in-situ heat treatment, which can harden Fe based alloys. This effect is underscored by the anisotropy seen in hardness values. In both specimens, the build direction orientation showed a significantly higher hardness than its corresponding build plane orientation. The build direction contains several thin layers of material, with fusion zones in between. Increased hardness in this orientation suggests that, in the same way a weld is often stronger than the material around it, these fusion zones are strong and the layers are therefore well adhered. While flake-shaped powders proved somewhat incompatible with L-PBF process parameters designed for spheroidal powders, this evidence of adhesion means that flakes can be made into solid parts, and it is a matter of process optimization.

Hardness measurements are used as a non-destructive method of evaluating the strength of a component with the values empirically lying between the yield and ultimate strength, depending on the work hardening nature of the material. Correlating hardness with ultimate tensile strength, the L-PBF specimen would be expected to have an ultimate strength between 75.7 ksi (along the build plane) and 111.4 ksi (in the build direction). The observed strength was slightly below the average of these two values. With these correlations thus validated, the tensile strength of LP-DED-11 can be approximated at 45.2 ksi, which is equivalent to a pure Fe specimen with 42% void content using the rule of mixtures approximation. In actuality, the

relative weakness can be a product of several factors, including void content, grain size, and residual thermal stresses.

Microstructural analysis reveals two notable phenomena. Firstly, Figure 11a shows observable anisotropy in the L-PBF specimen, which supports the different hardness values measured. LP-DED-11 does not appear to have the same degree of anisotropy (Figure 11b) and, as such, shows a smaller difference in hardness values between planes, despite having an overall larger spread. Secondly, the LP-DED specimen displays much smaller grains than those in L-PBF-1, indicating grain refinement during the manufacturing process. There are several factors that may lead to this difference in the two methods, but the end result is that LP-DED-11 underwent more in-situ normalizing than L-PBF-1, meaning that these processes may be used to achieve different properties as desired. While this study is not sufficient to claim that L-PBF manufacturing is best suited for flake-shaped powders, it can suggest the converse – flake morphology is more readily suited to L-PBF processing than to LP-DED. For LP-DED processing to achieve the same effectiveness with meteorite-extracted iron, there must be many more iterations of process optimization and likely more sophisticated pre-processing.

V. Further Study

As this is a preliminary study, many more variables and permutations must be evaluated before arriving at a meaningful conclusion. Work in the immediate future should focus on optimizing each process for its feedstock, and vice-versa, before directly comparing methods. To that point, there is a clear need for a higher-energy ball milling solution, or other technology to control metal powder morphology, for further evaluation of meteorite-extracted iron, such that the desired morphologies may be produced for each process. Additionally, just as this study seeks to look beyond established feedstock for additive manufacturing, there must be exploration of new and unique additive manufacturing methods for extra-terrestrial environments.

VI. Acknowledgements

Special thanks to Dr. Judy Schneider, my advisor, as well as Dr. Matt Marone of Mercer University, our collaborator in this work. Thanks to Dr. Bhaskar Dutta at DM3D Technology, Mr. Ken Cooper at NASA-MSFC, and Flacktek, Inc. for their contributions – without their equipment and expertise, none of this work would have been possible. Finally, thanks to the 2020 Honors Capstone Research Summer Program here at UAH for funding the bulk of this research.

Works Cited

Anderson, Iver E., Emma M.H. White, and Ryan Dehoff. "Feedstock powder processing research needs for additive manufacturing development." *Current Opinion in Solid State and Materials Science* 22 (2018): 8-15.

ASTM. *Standard Test Method for Flow Rate of Metal Powders Using the Hall Flowmeter Funnel.* Technical Standard, ASTM International, 2020.

ASTM. *Standard Test Methods for Determination of Carbon, Sulfur, Nitrogen, and Oxygen in Steel, Iron, Nickel, and Cobalt Alloys by Various Combustion and Inert Gas Fusion Techniques.* Technical Standard, ASTM International, 2018.

ASTM. *Standard Test Methods for Rockwell Hardness of Metallic Materials.* Technical Standard, ASTM International, 2020.

ASTM. *Standard Test Methods for Tension Testing of Metallic Materials.* Technical Standard, ASTM International, 2016.

Benjamin, J. S. "Mechanical Alloying." *Scientific American* 234, no. 5 (May 1976): 40-49.

Cleaves, Harold E., and John M. Hiegel. "Properties of High-Purity Iron." *Journal of Research of the National Bureau of Standards* 28 (May 1942): 643-667.

Field, A. C., L. N. Carter, N. J. E. Adkins, M. M. Attallah, M. J. Gorley, and M. Strangwood. "The Effect of Powder Characteristics on Build Quality of High-Purity Tungsten Produced via Laser Powder Bed Fusion (LPBF)." *Metallurgical and Materials Transactions A* 51A (March 2020): 1367-1378.

Fu, Xiaowei, Deborah Huck, Lisa Makein, Brian Armstrong, Ulf Willen, and Tim Freeman. "Effect of particle shape and size on flow properties of lactose powders." *Particuology* 10 (2012): 203-208.

Goh, Hui Ping, Paul Wan Sia Heng, and Celine Valeria Liew. "Comparative evaluation of powder flow parameters with reference to particle size and shape." *International Journal of Pharmaceutics* 547 (2018): 133-141.

MatWeb. *Iron, Fe.* http://www.matweb.com/search/DataSheet.aspx?MatGUID=654ca9c358264b5392d43315d8535b7d&ckck=1 (accessed August 18, 2020).

NASA. *NASA Technology Taxonomy.* 2019. https://www.nasa.gov/offices/oct/taxonomy/index.html (accessed November 15, 2019).

Rofman, O.V., A.S. Prosviryakov, A.V. Mikhaylovskaya, A.D. Kotov, A.L. Bazlov, and V.V. Cheverikin. "Processing and Microstructural Characterization of Metallic Powders Produced from Chips of AA2024 Alloy." *JOM* (The Minerals, Metals, & Materials Society) 71, no. 9 (June 2019): 2986-2995.

Yu, Weili, Koji Muteki, Lin Zhang, and Gloria Kim. "Prediction of Bulk Powder Flow Performance Using Comprehensive Particle Size and Particle Shape Distributions." *Journal of Pharmaceutical Sciences* 100, no. 1 (January 2011): 284-293.

Zocca, Andrea, Cynthia M. Gomes, Thomas Mühler, and Jens Günster. "Powder-Bed Stabilization for Powder-Based Additive Manufacturing." *Advances in Mechanical Engineering*, 2014: 1-6.